EPR Study of a Novel [Fe -Porphyrin] Catalyst

Yiannis Deligiannakis

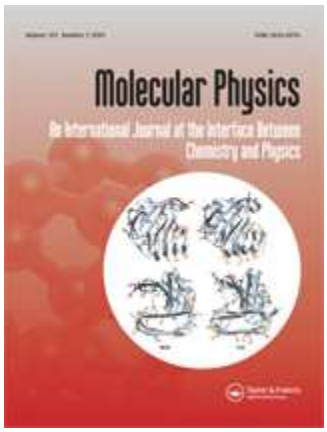

EPR Study of a Novel [Fe -Porphyrin] Catalyst

Journal:	*Molecular Physics*
Manuscript ID:	TMPH-2007-0154.R2
Manuscript Type:	Full Paper
Date Submitted by the Author:	03-Oct-2007
Complete List of Authors:	DELIGIANNAKIS, YIANNIS; University of Ioannina, Environmental & Natural Resources Management
Keywords:	EPR, Fe(IV)=O, porphyrin, catalysis, high valent iron

Christoforidis et. al. *11/7/2010* TMPH-2007-0154_Revised

EPR Study of a Novel [Fe -Porphyrin] Catalyst

KONSTANTINOS C. CHRISTOFORIDIS[a], MARIA LOULOUDI [b], ELENA R. MILAEVA[c], YIANNIS SANAKIS[d] & YIANNIS DELIGIANNAKIS [a*]

[a] *Dept of Environmental Natural Resources Management, Univ. of Ioannina, 30100 Agrinio, Greece.*

[b] *Dept. of Chemistry, University of Ioannina, 45110 Ioannina, Greece.*

[c] *Dept. of Organic Chemistry, Moscow State Lomonosov Univ. Moscow, 119992, Russia*

[d] *Inst. of Materials Science NCSR Demokritos 15310 Aghia Paraskevi Attikis Greece.*

Abstract

In this work we present an EPR and catalytic study of a novel [Fe-porphyrin] catalyst, [FeR_4P], used for the catalytic decomposition of pentacholorophenol (PCP). The porphyrin complex [FeR_4P] bears 2,6-di-*tert*-butylphenols (where R= di-Bu^{t}Phen) at each *meso*-aryl position of the porphyrin ring. The FeR_4P-SiO_2 catalyst was found to be very efficient for the degradation of PCP, using $NaIO_4$ as oxidant plus imidazole as cocatalyst. EPR spectroscopy shows that in the presence of the oxidant $NaIO_4$, at a redox potential of E_h=250mV, [FeR_4P] forms a high valent [Fe^{IV}=O $Por^{+\bullet}$] state with an EPR spectrum characterized by effective g-values $g_{\perp}^{eff} = 3.41$ and $g_{\parallel}^{eff} = 2$, similar to Compound I of Horseradish Peroxidase. The [Fe^{IV}=O $Por^{+\bullet}$] state can described by a S = 1 state of the oxoferryl Fe^{IV}=O weakly coupled by exchange interaction J to a S'=1/2 porphyrin cation radical. The zero field splitting of the Fe^{IV}=O is D= +16.5 K and the coupling parameters are J/D=0.31, J = +5.2 K. We suggest that the formation of [Fe^{IV}=O $Por^{+\bullet}$] specie to be the key intermediate responsible for the observed efficient catalytic decomposition of PCP.

Keywords Porphyrin, Catalysis**,** Ferryl, FeO(IV), High Valent Iron, Catalysis, chlorophenol, PCP, imidazole.

Corresponding Author: e-mail: ideligia@cc.uoi.gr

1. Introduction

Pentachlorophenol (PCP) has been used extensively as a fungicide, wood preservative, insecticide, and herbicide. Its broad use and environmental stability have led to the extensive contamination of soil, surface water, and groundwater aquifers [1, 2]. In this context, considerable research efforts have been dedicated for the development of efficient catalysts for the degradation of chlorophenols. For example, natural enzymes such as lignase, an extracellular peroxidase produced by white rot fungus *Phanarochaete chrysosporium*, is able to degrade PCP [3, 4]. In another approach, to mimic the oxidative transformation of chlorophenols, including PCP, by lignase and/or peroxidases, extensive studies using biomimetic iron(III)-porphyrin complexes (Por-Fe^{III}) have been conducted [5-9].

In general, among the key features of the design of an efficient catalyst is its protection against oxidative deactivation due to the rapid self-oxidation [10, 11]. In this context, it is well known that the oxidative stability of metallo-tetra-aryl-porphyrins is affected by the presence of substituents on the porphyrin ring. In this context the presence of bulky substituents at the *ortho*-positions of the aryl groups has been shown to enhance stability against oxidative degradation[12]**.** For example, the tetrakis(2,6-dichloro- and 2,6-dibromo-phenyl) porphyrins have been shown to be effective and robust catalysts [13-15]. It is generally accepted that this increased stability towards oxidative self-destruction arises from a combination of the electron-withdrawing polar effects but also on the steric hindrance of the substituents [13-15].

Model systems that mimic the catalytic center of enzymes have been synthesized and studied extensively [10, 12, 16]. In such systems, oxoiron(IV) species, [Fe^{IV}=O], are typically invoked as the reactive intermediates in heme-iron dependent oxygenases [10, 12, 16]. One goal of such studies has been the characterization of these high-valent iron-oxo species that are responsible for the oxidation of various organic substrates both *in vivo* and *in vitro* [12, 16]. Typically, in the catalytic cycle two intermediates i.e. known as Compound I and Compound II, can be formed, both containing the high valent ferryl [Fe^{IV}=O] moiety. In Compound I, the porphyrin is also oxidized to a radical state, forming an oxoferryl porphyrin π-cation radical [Fe^{IV}=O $Por^{+\bullet}$]. Thus Compound I which is characterised by a

characteristic green colour, is a product of a two-electron oxidation of the [Fe-porphyrin] center. Compound II which is red is the one electron reduction of Compound I [12, 16].

Electron Paramagnetic Resonance (EPR) has been widely used to characterize the catalytic cycles and to identify the intermediate oxidative species in enzymes and model compounds [17-22]. The oxo-iron porphyrin π-cation radical [Fe^{IV}=O $Por^{+\bullet}$] similar to the Compound I of Horseradish Peroxidase (HRP) is accepted by most researchers as the oxenoid intermediate observed in model systems [23]. This specie is characterized by a broad EPR signal derived from a S=1 oxoferryl moiety weakly coupled with an S'=1/2 porphyrin cation radical. This interaction was first proposed by Schulz *et al*. [18] to explain the EPR signal centered at g ~ 2 for HRP Compound I. Subsequent ENDOR experiments confirmed that the broad EPR signal is associated with the porphyrin radical [24]. Furthermore, by using $H_2{}^{17}O_2$ these studies showed that an oxygen atom from $H_2{}^{17}O_2$remains bound to the iron atom of HRP Compound I [24]. Its green color and the decrease in absorbance of the Soret band have also been used to identify this species with UV-Vis spectroscopy in model systems [25].

Here we present a combined EPR and catalytic study of a novel [Fe-porphyrin] catalyst used for the catalytic decomposition of pentacholorophenol (PCP). The porphyrin complex [FeR_4P] bears 2,6-di-*tert*-butylphenols (where R=di-Bu^{t}Phen) at each *meso*-aryl position of the porphyrin ring. Moreover, a heterogenised FeR_4P-SiO_2 catalyst was synthesized by covalent attachment of FeR_4P onto functionalized silica *via* an imidazole. The catalysts, homogeneous and heterogeneous, were evaluated for the degradation of PCP. Immobilization of the catalyst on silica support is advantageous in industrial processes by facilitating both catalyst separation and recycling, and also by reducing effluent contamination. Immobilization also ensures that only monomeric complexes are responsible for the degradation of the substrate.

The main aim of the present work is to study by EPR the reactive species formed during the redox steps involved in the catalytic cycle. Finally the structural information obtained by EPR, is discussed in conjunction with the catalytic results.

2. Experimental Section

All solvents and reagents were of commercial grade unless otherwise stated and were purchased from Merck and Aldrich.

Metalloporphyrin: The porphyrin **A**, see Scheme 1**,** was synthesized by known procedures as described previously [26, 27] and purified by silica gel column chromatography using $CHCl_3$, 80 % $CHCl_3$ and 20 % hexane as the eluting solvents.

Immobilization: Immobilization of the metalloporphyrin **A** was achieved using a procedure described in detail previously [28]. The process is: modified imidazole 3-(glycidyloxypropyl) silica (IGOPS), was obtained using the procedure described previously [28]: 3-(glycidyloxypropyl)-trimethoxysilane (3 mmol; 0.663 ml) was added to a stirred solution of imidazole (3 mmol; 0.204 g) in 50 ml of toluene. The resulting mixture was heated at 80 ^{o}C for 24 h, and after drying commercial SiO_2 (1.5 g) and EtOH (5 ml) were added. The reaction mixture was then stirred at 80 ^{o}C for 24 h. The functionalized silica IGOPS was collected by filtration in vacuum and washed with EtOH and $(CH_3)_2O$. IGOPS was dried for 12 h. The loading achieved is 20% determined by thermogravimetric and elemental analysis [29]. The metalloporphyrin ligation to IGOPS was achieved by stirring a CH_2Cl_2 solution of a known amount of metalloporphyrin into a suspension of the support for 24 h. The resulting supported catalyst, herein called **B**, was washed with CH_2Cl_2 to remove unbound catalyst and weakly bound porphyrin and dried for 3 h at 60°C. The loadings were quantified by measuring the amount of unloaded metalloporphyrin in the combined reaction solvent and washings by UV-Vis spectroscopy.

EPR Spectroscopy: Electron Paramagnetic Resonance (EPR) spectra were recorded with a Brucker ER200D spectrometer at liquid He or liquid N_2 temperatures, equipped with an Agilent 5310A frequency counter. The spectrometer was running under a home-made software based on LabView. For the quantification of the signals the second integral of the EPR spectra was used. Progressive EPR saturation data were collected by measuring the EPR absorption derivative signal intensity as a function of progressive increase of the microwave power at different temperatures. The saturation data were fit by using the expression

$$S / P^{1/2} \propto 1/(1 + P / P_{1/2})^{1/2} \quad (1)$$

where S is the derivative signal intensity, P is the microwave power, and $P_{1/2}$ is the half-saturation power. A nonlinear least-squares fit to the above equation yielded a $P_{1/2}$ value at each particular temperature.

UV-Vis spectroscopy: Light absorbance spectra in the ultraviolet-visible region (190-900nm) were recorded by using a double-beam Perkin-Elmer Lambda-35 UV-Vis spectrophotometer with 10mm quartz cells.

HPLC: Quantitative HPLC determinations for PCP were performed with a Dionex P680 HPLC chromatograph equipped with a Dionex 1024 Diode Array Detector. The column used was Acclaim C18 5μM, 120Å, 4.6x250mm and was thermostated at 23°C. The HPLC mobile phase was 85% acetonitrile and 15% (Milli-Q) water plus 0.8% H_3PO_4 with a flow rate of 1 ml/min.

'[Insert Scheme 1 about here]'

EPR Sample preparation: Homogeneous FeR_4P solutions 6mM were prepared in CH_2Cl_2. Then, for the preparation of the 1:1 [**A**:Imidazole] sample, 10μl of 60mM imidazole aqueous stock solution was added in 90μl of **A** in CH_2Cl_2. Similarly, for the preparation of the 1:10 [**A**:Imid] sample, 10μl of 600mM imidazole aqueous stock solution was added in 90μl of **A** in CH_2Cl_2 60mM. For the oxidation of the samples, $NaIO_4$ was used as oxidant. Two samples were prepared with either 28 mM or 14 mM of $NaIO_4$ (10μl or 5μl of 280mM $NaIO_4$ aqueous stock solution respectively i.e. 4.7 or 2.3 equivalents of $NaIO_4$ respectively per Fe-Por.).

For the SiO_2 supported FeR_4P, 54μl of CH_2Cl_2, were added to 5mg of the heterogenised complex (i.e. 1mM **A**), then either 10 or 1mM of imidazole (i.e. 10 or 1 equivalents of imidazole per **A**) was added. For the oxidation of the sample 28 mM or 14 mM of $NaIO_4$ were added in the two samples followed by incubation at 25 °C for up to 30 minutes. Then the samples were frozen at 77K and measured by EPR. We found that this time span was adequate for accomplishment of the observed changes in EPR spectra.

UV-Vis Sample preparation: Samples were prepared in 10mm quartz cells. A typical reaction mixture contained 2.965ml of acetonitrile (CH_3CN), 5μl of 6mM stock solution of 10μM **A** in CH_2Cl_2 plus 100 or 10μM of imidazole (i.e. 10 or 1 equivalents of imidazole respectively with respect to the complex **A**) and 10μM of $NaIO_4$ (i.e. 1 equivalent of $NaIO_4$ with respect to the FeR_4P complex). In all samples, appropriate volumes of Milli-Q water were added to a final ratio [CH_3CN:H_2O] of [100:1].

Catalytic Experiments: All reactions were performed in test tubes of 4 ml volume equipped with a magnetic stirrer at room temperature. A typical reaction mixture contained 187.5 μM PCP (100 μl of a 3.75 mM acetonitrile stock solution), 18.7 μM of the catalyst (0.0032 g of the immobilized or 207.7 μl of a 180 μM acetonitrile stock solution of the homogeneous catalyst i.e. [catalyst : substrate] = [1:10]), 2.34 mM of the oxidant (23.4 μl of a 200 mM $NaIO_4$ aqueous stock solution i.e. 125 equivalents of oxidant with respect to the substrate), 187 μM of imidazole as co-catalyst (37.4 μl of 10mM aqueous stock solution i.e. 10 equivalents of imidazole with respect to the catalyst). For all reactions tested, the appropriate volumes of acetonitrile and milli-Q water were added so that the final volume of the reaction was 2 ml and the ratio [acetonitrile:H_2O] = [3:1], v/v, unless otherwise mentioned. We selected this solvent mixture [acetonitrile:H_2O] [3:1] because FeR_4P is only soluble in non-polar solvents. Acetonitrile was also used as co-solvent to solubilize the hydrophobic PCP. The solubility of PCP in H_2O is limited (52.5 μM). On the other hand, imidazole and $NaIO_4$ are more soluble in H_2O. In all cases the oxidant was the last reagent added. The quantification of PCP by HPLC was based on comparison with standards.

3. Results and discussion

3.1 Catalytic activity

Kinetic results for the catalytic degradation of PCP are displayed in Figure 1, for the homogeneous **A** (solid symbols) or the heterogeneous **B** (open symbols) catalyst, respectively. As shown in Figure 1, the decomposition of PCP by catalyst **A** attained a maximum near 60%, i.e. 40% of PCP remaining, within ~8 hours. On the other hand, the heterogenised catalyst **B** decomposed 100% of PCP within 130 minutes, Figure 1. Catalyst **B** could be easily recovered by centrifugation and reused. Repetitive uses showed that catalyst **B** was highly recyclable i.e. 100% PCP decomposed after a second usage of the same FeR_4P-SiO_2 and 30% after a third usage.

'[Insert Figure 1 about here]'

Overall, the catalytic data presented in Figure 1 show that FeR_4P can catalyse the decomposition of PCP. Moreover, the heterogenised FeR_4P-SiO_2 is more efficient than the homogeneous catalyst. Detailed kinetic and product analysis data will be presented in a separate paper. Here, in an effort to better understand the reactive species formed during the catalytic cycle, we focus on EPR spectroscopic data.

3.2 EPR Spectroscopy

3.2.1 High to Low Spin Fe^{III} conversion. The EPR spectrum of **A** in CH_2Cl_2, Figure 2A(a), is characterised by an axial EPR signal of High Spin (HS) Fe^{III}(S=5/2) with g_x= 6.13, g_y=5.77, g_z=1.99 typical for high spin porphyrin-Fe^{III} complexes [29]. Based on the g_x, g_y values a E/D rhombicity ratio of 0.013 is estimated.

'[Insert Figure 2 about here]'

After addition of 1 equivalent of imidazole per Fe, the intensity of the HS Fe^{III}(S=5/2) EPR signal is diminished with no other spectral changes, see Figure 2A(b). The signal could be fully recovered by reoxidation, by $NaIO_4$ (data not

shown). This indicates that the effect of 1 equivalent of imidazole per Fe, seen in Figure 2A(b) is due to reduction of the iron, most likely to the ferrous Fe^{II} state [30].

In another sample, addition of 10 equivalents of imidazole results per Fe, has a totally different effect i.e. converts the iron to the Low Spin (LS) Fe^{III}(S=1/2) state, [30, 31]. This can be seen in Figure 2A(c). The detailed time dependence of the HS to LS conversion is shown in Figure 3. The kinetics is rather rapid with a $t_{1/2}$ near 100 seconds, see Figure 3. 100% conversion of the initial S = 5/2 Fe^{III} to the Low Spin state, is accomplished after 8 min of incubation. We underline that no radical signal was present in these samples.

'[Insert Figure 3 about here]'

3.2.2 g-values of Low Spin Fe^{III}. The g values of the LS signal are listed in Table 1. Two conformers of the LS Fe^{III} signals are resolved with slightly different g tensors herein called LS^A and LS^B (LS^A: g_x = 2.858, g_y = 2.305, g_z = 1.56 and LS^B: g_x = 2.850, g_y = 2.285, g_z = 1.60), see Table 1. The relative intensities of these two species were found to vary between different samples, however both were present in all samples tested. The rhombic g-values are typical for two imidazoles axially coordinated in low spin Fe^{III} [32]. Moreover the g values might be taken as indication that the planes of two axially coordinated imidazoles aligned approximately parallel to one another, confirmed by continuous wave [31, 33] as well as by pulsed EPR spectroscopy [34].

In Table 1, the g-values as well as the rhombicity (V/Δ) and tetragonality (Δ/λ) parameters i.e. calculated from the g-values, are compared with pertinent literature data. In low spin ferrihemes and ferriheme proteins, Peisach and Blumberg noticed that the V/Δ and Δ/λ values can provide evidence on the nature of the axial ligands [35]. Accordingly, the two forms of Low Spin Fe^{III} signals observed for **A**$(Imid)_2$ can be explained by the formation of two different **A**$(Imid)_2$ molecules, both having the imidazole ligands in parallel planes, but different angle φ between the closest N_P–Fe–N_P axis and the projection of the imidazole planes [33]. The signal with smaller tetragonality and larger rhombicity (LS^A), see Table 1, arises from the molecules with small angle φ while the signal with larger tetragonality and smaller rhombicity (LS^B) arises from those having larger angle φ [33].

'[Insert Table 1 about here]'

3.2.3 High valent-iron species. After formation of the low spin form, sample **A** was oxidised by $NaIO_4$. Within 15 minutes after addition of the oxidant the low spin EPR signal intensity decreased near zero, with a concomitant development of a broad signal with a sharp feature near *g*=2, see Figure 2A(d). The new signal contained a derivative radical-like feature with a zero-crossing point at *g*=2.0049 and ΔH=25G, accompanied by broad flanks with a bump at g=3.41, see inset in Figure 2A. As we show in the following, this signal can be assigned to a oxo-Fe^{IV} porphyrin π-cation radical [Fe^{IV}=O $Por^{+\bullet}$].

The spectral changes are easier to observe in the first integral of the EPR spectra, see Figure 2B. The broad signal is developed at the expense of the low-spin signal, attaining maximum intensity after 20 minutes see Figure 4. A close inspection of Figure 4, reveals that the decay of the LS Fe^{III} signal has $t_{1/2}$~8 minutes, while the $t_{1/2}$ of the broad signal is $t_{1/2}$ ~15minutes. This indicates that the formation of the broad signal requires additional steps, probably formation of an EPR silent intermediate species through the oxidation of the homogeneous **A** complex. Incubation of the oxidized sample for more than 20min results to a decrease of the broad signal, see Figure 4.

'[Insert Figure 4 about here]'

3.3 UV-Vis spectroscopy

Concomitant with the EPR changes shown in Figures 2, the oxidation of sample **A** resulted in a gradual colour change from purple to green. This can be seen in the absorption spectra for the **A** sample, in Figure 5. Upon addition of imidazole in a ratio [imidazole:**A**]=[10:1] the shoulder at 375nm and the peak at 514nm, disappeared. These features can be attributed to Cl^- coordination to the Fe-Por [36, 37]. When we used 1 equivalent of imidazole only 10% of these two signals disappeared (data not shown).

'[Insert Figure 5 about here]'

Upon oxidation of the sample with 1 equivalent of $NaIO_4$ per **A**, a decrease of the Soret band was observed and a well defined band at the visible area was generated at 665nm, see inset in Figure 6. We also notice a blue-shift of the Soret band of about 2nm. All these changes in the visible spectrum are characteristic for the formation of a ferryl porphyrin π-cation radical [38, 39]. This green colour at 665nm is characteristic of the formation of oxo-Fe^{IV} porphyrin π-cation radical (ferryl porphyrin π-cation radical, (Fe^{IV}=O $Por^{+\bullet}$) [37, 40, 41].

'[Insert Figure 6 about here]'

3.4 Spin Hamiltonian parameters

The EPR [Fe^{IV}=O $Por^{+\bullet}$] signal of **A** is displayed in Figure 6. This signal bears relevance to previously reported EPR spectra of heme enzymes [17-20, 24] or model Fe-Porphyrin systems [21,22] under comparable conditions. Accordingly, this EPR signal is derived from a S=1 oxoferryl moiety magnetically coupled to a S'=1/2 porphyrin cation radical [17-24]. The magnetic coupling is determined by both exchange and dipolar terms [18, 24]. This coupling scheme was first proposed by Schulz *et al*. [18] to explain the EPR signal centered at g~2 for Horseradish Peroxidase Compound I. Subsequent ENDOR experiments confirmed that the broad EPR signal is associated with the porphyrin radical [24]. Since the first works [18, 24] analogous EPR spectra were discovered and interpreted analogously in Lignin Peroxidase [17], and Chloroperoxidase [20] as well as in oxidation reactions of $FeTM(4)PyP^{5+}$ with iodosylbenzene [21, 22]. Of immediate relevance to our results is the work of Fujii et al. [42] for substituted Fe-porphyrins in organic solvent [42]. Oxidation of these Fe-porphyrins substituted at the pyrole carbons produced [Fe^{IV}=O $Por^{+\bullet}$] EPR signals [42] similar to those shown in Figure 2 for **A**.

The EPR signals can be interpreted by assuming a weakly coupled pair of spins Fe^{IV}=O(S=1) and $Por^{+\bullet}$(S'=1/2). The coupling is assumed to be a weak exchange interaction J [18, 24, 42]. Within the formalism of the weakly coupled (S=1 and

S'=1/2) system, the [Fe^{IV}=O $Por^{+\bullet}$] is characterised by three Kramer's doublets separated by energy gaps which are mainly determined by the value of *D,* that is the zero-field splitting of the *S*=1 state of Fe^{IV}=O [18, 24]. Since for the ferryl porphyrin center *D* is expected to be greater than zero [18, 24, 42], a value for $g_{\perp}$ that is greater than $g_{||}$ results from ferromagnetic coupling [24, 42].

$$g_{\perp} > g_{||} \qquad J > 0 \text{ (ferromagnetic coupling)}$$

In this coupling scheme, for weak couplings, $|J| << D$, the ground doublet which is responsible for the observed EPR signal, is separated from the excited states by an energy $\Delta E \sim D$, see inset in Figure 7. Since phonon-induced transitions within a doublet are forbidden in first order, spin relaxation is dominated by Orbach processes via excited states. In such systems, the temperature dependence of the spin-lattice relaxation rate (1/*T*) can provide an estimate of the energy separation between the ground from the excited states (ΔE) [24, 42]. The spin relaxation is dominated by Orbach processes *via* excited doublet states at all but the lowest temperatures. Figure 7 shows the logarithm of the half-saturation power $P_{1/2}$, which is defined in eq. (1), as a function of *1/T*. The data in Figure 7 were fitted by the function

$$P_{1/2} \sim AT + B / \left[e^{\frac{\Delta E}{T}} - 1 \right] \qquad (2)$$

with

$$\Delta E = 13.4 \pm 2.0 \text{ K } (9.4 \pm 0.6 \text{ cm}^{-1})$$

'[**Insert Figure 7 about here**]'

The value of $g_{\perp}^{eff}$ is determined by the exchange interaction with the ferryl moiety (*S* = 1). To a first approximation [24, 42]

$$g_{||}^{eff} \sim g_e$$

$$g_{\perp}^{eff} \sim g_e + 2g_{\perp}^{Fe}(J/D) \qquad (3)$$

where $g_{\perp}^{Fe}$ is associated with the isolated [Fe^{IV}= O]$^{2+}$ moiety and can be taken equal to 2.25 [43] and *J/D* is the ratio of exchange coupling to the zero-field splitting

parameter of $[Fe^{IV}= O]^{2+}$. For complex **A** the g values were taken from the EPR spectrum, Figure 6

$$g_{\perp}^{eff} = 3.41$$

and

$$g_{\parallel}^{eff} \sim 2$$

Then, using eq. (3) these g-values, give

$$\frac{|J|}{D} = 0.31 \qquad (4)$$

with J>0 i.e. ferromagnetic coupling. The ratio J/D = 0.31 is close to that estimated by Fujii et al [42] for their substituted Fe-Por. model compounds **1-4** [42]. Accordingly, for a J/D=0.31 the value of ΔE is ~ 0.8 D [42] therefore

$$D = \frac{\Delta E}{0.8} = \frac{13.4}{0.8} = +16.7 \text{ K} \quad (+11.5 \text{ cm}^{-1}) \qquad (5)$$

And, using (4)

$$J = +5.2\text{K } (+3.6 \text{ cm}^{-1}) \qquad (6)$$

The estimated Spin Hamiltonian parameters for **A** are summarized in Table 2, together with pertinent reference data from the literature.

'[Insert Table 2 about here]'

4. Discussion

Both EPR as well as Visible absorption spectra indicate that high valent Fe species are formed by oxidation of **A** by $NaIO_4$. The high valent specie is responsible for the formation of a ferryl porphyrin π-cation radical, Fe^{IV}=O $Por^{+\bullet}$, state. Though a detailed redox titration of the various intermediates detected by EPR and UV-Vis have not been done, we notice that the redox potential of E_h=+250mV created by the added $NaIO_4$ in our experiments was adequate for formation of the [Fe^{IV}=O $Por^{+\bullet}$] state in the majority of the centres. Control experiments with free-base R_4PH_2 porphyrin in various aprotic organic solvents, showed that no radical is formed under redox potentials up to 250mV, posed by $NaIO_4$. This is because in aprotic organic solvent i.e. such as CH_2Cl_2 in the present case, the tert-butyl phenols of catalyst **A** remain always protonated which in turn prohibits formation of phenoxyl radicals.

From Table 2 we observe that the *J/D* ratio in **A** is comparable with the value for compound **1** of Fujii et al [42] and ASP [44]. Noticeably, however, the dipolar coupling value *D* in **A** is smaller i.e. by 40%, than the *D* value of compound **1** of Fujii et al [42] and ASP [44]. A more detailed discussion in geometrical terms is difficult to be done, with the data at hand. The variety of *J/D*, *D* and *J* values reported in the literature, see Table 2, originates from the fact that the *J* and *D* values are determined from weak interactions, which are sensitive to orbital symmetry [42], which in turn is influenced by local effects such as ring substituents [42] but also on the axial ligands [45]. In the case of **A** the axial ligands in the [Fe^{IV}=O $Por^{+\bullet}$] are not known, however we consider that at least one imidazole should be axially coordinated. This argument is based on the fact that imidazole is coordinated axially to iron in the low-spin Fe^{III} state, see discussion in paragraph *g-values Low-Spin Fe^{III} signals* above.

4.1 Role of [Fe^{IV}=O $Por^{+\bullet}$] in PCP catalysis

The high–valent iron–oxo species are generally accepted as being responsible for the oxidation of several organic substrates by heme enzymes and model compounds [12, 16]. In the catalytic cycles of several peroxidases and catalases it has been suggested that a common mechanistic step involves oxidation of Fe^{III} to high–valent Fe^{V}

oxidation state [46]. In heme systems, two key intermediates [Fe^{IV}=O $Por^{+\bullet}$] (Compound I) and [Fe^{IV}=O] (Compound II) can be formed [46]. Horseradish peroxidase [47] and Lignin peroxidase [48] have been known to oxidise polychlorinated phenols through the formation of Compound I and II [12, 16, 47]. Our data indicate that the [Fe^{IV}=O $Por^{+\bullet}$] state can be formed under the conditions used for the catalysis of PCP. Taking into account the mechanistic role of [Fe^{IV}=O $Por^{+\bullet}$] specie in catalytic reactions [12, 16, 47] we may suggest that the observed efficient catalysis of PCP by catalyst **A** involves the [Fe^{IV}=O $Por^{+\bullet}$] specie. Therefore, in our systems we suggest that the formation of a [Fe^{IV}=O $Por^{+\bullet}$] state in catalyst **A**, which is highly reactive, is involved as a catalytic reaction intermediate, in the observed catalytic degradation of PCP.

In the same context, we recall that among the key features of the design of an efficient catalyst is its protection against oxidative deactivation due to the rapid self-oxidation [10, 11]. For example, it is well known that the oxidative stability of metallo-tetra-aryl-porphyrins is affected by the presence of substituents on the porphyrin ring as the presence of bulky substituents on the *ortho*-positions of the aryl groups [12]**.** In this respect, tetrakis(2,6-dichloro- and 2,6-dibromo-phenyl) porphyrins have been shown to be effective and robust catalysts [13-15]. It is generally accepted that this increased stability towards oxidative self-destruction arises from a combination of the electron-withdrawing polar effects but also on the steric hindrance of the substituents [13-15].

Accordingly we would like to highlight that the heterogenised A-SiO_2 catalyst can be reused at least three times, under the oxidizing conditions of our catalytic experiments. This enhanced stability of the catalyst can be attributed to the protective effect of the bulky 2,6-di-*tert*-butylphenols as well as the SiO_2 matrix.

5. Conclusions

EPR and Visible absorption spectra indicate that high valent Fe species are formed by oxidation of **A** by $NaIO_4$ at E_h=250mV. The EPR data show that a high valent [Fe^{IV}=O $Por^{+\bullet}$] state is formed similar to Compound I of Horseradish Peroxidase. The zero field coupling parameters *J* and *D* have been determined for the spin couple

[Fe^{IV}=O (*S*=1)] and [$Por^{+\cdot}$ (*S*′=1/2)]. The *J/D* value for **A** is comparable with certain literature data, however the individual *J* and *D* values are the smallest reported so far. Structure and geometry details are the determinant factors. This calls for a need for more systematic investigation by pertinent model systems, together with quantum chemical calculations.

Acknowledgment: This work has been supported by a Greek-Russia bilateral collaboration project funded by the General Secretariat for Research and Technology (GGET).

References

[1] D. F. Goerlitz, D. E. Troutman, E. M. Godsy, B. J. Franks. *Environ. Sci. Technol.*, **19**, 955 (1985).

[2] R. Valo, V. Kitunen, M. S. Salkinoja-Salonen, S. Raisanen. *Chemosphere*, **13**, 835 (1984).

[3] G. J. Mileski, J. A. Bumpus, M. A. Jurek, S. D. Aust. *Appl. Environ. Microbiol.*, **54**, 2855 (1988).

[4] C. Ruttimann-Johnson, R. T. Lamar. *Soil Biol. Biochem.*, **29**, 1143 (1997).

[5] S. Hasan, J.-G. Cho, K. L. Sublette, D. Pak, A Maule. *J. Biotechnol.*, **24**, 195 (1992).

[6] G. Labat, J.-L. Seris, B. Meunier. *Angew. Chem., Int. Ed. Engl.*, **29**, 1471 (1990).

[7] R. S. Shukla, A. Robert, B. Meunier. *J. Mol. Catal. A*, **113**, 45 (1996).

[8] M. Fukushima, H. Ichikawa, M. Kawasaki, A. Sawada, K. Morimoto, K. Tatsumi. *Environ. Sci. Technol.*, **37**, 1031 (2003).

[9] M. Fukushima, A. Sawada, M. Kawasaki, H. Ichikawa, K. Morimoto, K. Tatsumi, M. Aoyama. *Environ. Sci. Technol.*, **37**, 386 (2003).

[10] R. A. Sheldon, (Ed.), *Metalloporphyrins in Catalytic Oxidations*; Marcel Dekker: New York, 1994.

[11] M. J. Nappa, C. A. Tolman. *Inorg. Chem.*, 24, 4711 (1985).

[12] B. Meunier. *Chem. Rev.*, **92**, 1411 (1992).

[13] P. S. Traylor, D. Dolphin and T. G. Traylor. *J. Chem. Soc., Chem. Comm.*, **5**, 279 (1984).

[14] D. Ostovic, T. C. Bruice. *J. Am. Chem. Soc.*, **111**, 6511 (1989).

[15] M. D. Assis, J. R. L. Smith. *J. Chem. Soc*., *Perkin Trans. II*, 10, 2221 (1998).

[16] D. Mansuy. *Coord. Chem. Rev.*, **125**, 129 (1993).

[17] A. Khindaria, A. D. Aust. *Biochemistry*, **35**, 13107 (1996).

[18] C. E. Schulz, P. W. Devaney, H. Winkler, P. G. Debrunner, N. Doan, R. Chiang, R. Rutter, L. P. Hager. *FEBS Lett.*, **103**, 102 (1979).

[19] C. E. Schulz, R. Rutter, J. T. Sage, P. G. Debrunner, L. P. Hager. *Biochemistry*, **23,** 4743 (1984).

[20] R. Rutter, L. P. Hager, H. Dhonau, M. Hendrich, M. Valentine, P. Debrunner. *Biochemistry*, **23**, 6809 (1984).

[21] S. Nagakaki, Y. Iamamoto, O. Baffa, O. R. Nascimento. *Inorg. Chim. Acta*, **186**, 39 (1991).

[22] Y. Iamamoto, M. das D. Assis, O. Baffa, S. Nakagaki, O. R. Nascimento. *J. Inorg. Biochem.*, **52**,191 (1993).

[23] J. T. Groves, R. Quinn, T. J. McMurray, M. Nakamura, G. Lang, B. Bose. *J. Am. Chem. Sot.*, **107**, 354 (1985).

[24] J. E. Roberts, B. M. Hoffman, R. Rutter, L. P. Hager. *J. Am. Chem. Soc.*, **103**, 7654 (1981).

[25] C. K. Chang, M-S. Kuo. *J. Am. Chem. Soc.*, **101**, 3413 (1979).

[26] L.R. Milgrom, C.C. Jones, A. Harriman. *J. Chem. Soc. Perkin Trans II.*, **1**, 71, (1988).

[27] T.G. Traylor, K.B. Nolan, R. Hildreth. *J. Am. Chem. Soc.*, **105**, 6149 (1983).

[28] M. Louloudi, K. Mitopoulou, E. Evaggelou, Y. Deligiannakis, N. Hadjiliadis, *J. Mol. Catal. A: Chem.*, **198**, 231 (2003).

[29] B. J. Gaffney, H. J. Silverstone, In *Biological Magnetic Resonance "EMR of Paramagnetic Molecules"*, L. J. Berliner, J. Reuben (Eds.), vol. 13. pp 1-55, Plenum Press, New York, (1993).

[30] M. L. Kennedy, S. Silchenko, N'vida Houndonougbo, B. R. Gibney, P. Leslie Dutton, Kenton R. Rodgers, and David R. Benson *J. Am. Chem. Soc.***, 123**, 4635 (2001).

[31] F. A. Walker, D. Reis, V. L. Balke, *J. Am. Chem. Soc.*, **106**, 6888 (1984).

[32] D. R. Benson, B. R. Hart, X. Zhu, M. B. Doughty, *J. Am. Chem. Soc.*, **117**, 8502 (1995).

[33] F. A. Walker, B. H. Huynh, W. R. Scheidt, S. R. Osvath. *J. Am. Chem. Soc.*, **108**, 5288 (1986).

[34] E. Vinck, S. Van Doorslaer. *Phys. Chem. Chem. Phys*., **6**, 5324 (2004).

[35] J. Peisach, W. E. Blumberg, A. D. Adler. *Ann. N.Y. Acad. Sci.*, **206**, 310 (1973).

[36] C.M.C.P. Mans, C.R. Neri, E.A. Vidoto, H.C. Sacco, K.J. Ciuffi, L.S. Iwamoto, Y. Iamamoto, O.R. Nascimento, O.A. Serra. *J. Inor. Biochem.*, **73**, 85 (1999).

[37] W. Nam, M. H. Lim, S-Y. Oh. *Inorg. Chem.*, **39**, 5572 (2000).

[38] J. T. Groves, R. C. Haushalter, M. Nakamura, T. E. Nemo, B. J. Evans. *J. Am. Chem. Soc.*, **103**, 2884 (1981).

[39] M.D. Assis, O. A. Serra, Y. Iamamoto, O. R. Nascimento. *Inorg. Chim. Acta*, **187**, 107 (1991).

[40] R. H. Felton, G. S. Owen, D. Dolphin, J. J. Fajer. *J. Am. Chem. Soc.*, **93**, 6332 (1971).

[41] R. H. Felton, G. S. Owen, D. Dolphin, A. Forman, D. C. Borg, J. Fajer. *Ann. N. Y. Acad. Sci.*, **206**, 504 (1973).

[42] H. Fujii, T. Yoshimura, H. Kamada. *Inorg. Chem.*, **35**, 2373 (1996).

[43] B. M. Hoffman, J. E. Roberts, C. H. Kang, E. Margoliash. *J. Biol. Chem.*, **256**, 6556 (1981).

[44] W. R. Patterson, T. L. Poulos, D. B. Goodin. *Biochemistry*, **34**, 4342 (1995).

[45] M. J. Benecky, J. E. Frew, N. Scowen, P. Jones, B. M. Hoffman. *Biochemistry*, **32**, 11929 (1993).

[46] Meunier B. (ed.) *Structure and Bonding: Metal-Oxo and Metal Peroxo Species in Catalytic Oxidation* Springer-Verlag, Berlin (2000).

[47] R. P. Ferrari, E. Laurenti, F. Trotta. *J. Inorg. Biol. Chem.*, **4**, 232 (1999).

[48] K. E. Hammel, P. J. Tardone. *Biochemistry*, **27**, 6563 (1988).

[49] M. Ikeda-Saito, T. Iizuka. *Biochim. Biophys. Acta*, **393**, 335 (1975).

[50] H. Hori. *Biochim. Biophys. Acta*, **251**, 227 (1971).

Figure Captions

Scheme 1 (**A**) *meso*-tetra(3,5-di-*tert*-butyl-4-hydroxyphenyl) iron porphyrin (FeR_4P) catalyst and (B) supported on SiO_2 (FeR_4P-SiO_2).

Figure 1 Catalytic decomposition of PCP using the homogenised **A** (!) and the heteroganised **B** (∀) catalyst. Catalytic conditions as mentioned above Catalytic conditions [catalyst:Imidazole:PCP:$NaIO_4$] =[1:10:10:125].

Figure 2 A) First derivative EPR spectra of 6mM **A.** a) in CH_2Cl_2 b) incubated for 30min with 6mM imidazole and c) incubated for 30min with 60mM imidazole and d) 30min with 28mM $NaIO_4$. Inset plot zoom of spectrum d. B) Absorption EPR spectra obtained by numerical integration of the spectra (a), (c) and (d) respectively in panel (A). EPR conditions, Temperature 4.2K, modulation amplitude 10G, modulation frequency 100KHz, microwave power 0.7mW.

Figure 3 Time dependence of the high spin (!) to low spin (∀) Fe^{III} conversion of the **A** complex (6mM **A** and 60mM imidazole).

Figure 4 Time dependence of the LS **A**$(Imid)_2$ (!) and the g = 2.0049 (∀) signal after addition of 28mM $NaIO_4$. For the quantitation, the peak intensities of the low field low spin Fe^{III} and the g = 2.0049 signal were used.

Figure 5 Visible spectra of the 10μM of A in CH_3CN (doted line), incubated with 10 equivalents of imidazole for 10min (dashed line), incubated with one equivalent of $NaIO_4$ for 10min (dashed dot line, green solution) and 20min (solid line, green solution).

Figure 6 Complex **A**$(Imid)_2$ after incubation for 30min with 28mM $NaIO_4$. EPR conditions, Temperature 4.2K, modulation amplitude 10G, modulation frequency 100KHz, microwave power 0.7mW.

Figure 7 Half-saturation power, $P_{1/2}$ of the g = 2.0049 EPR signal of catalyst **A** as a function of temperature. The dashed line is a best fir using equation (2) for ΔE= 13.4 K, and Orbach coefficients A=0.05, B=17.57.

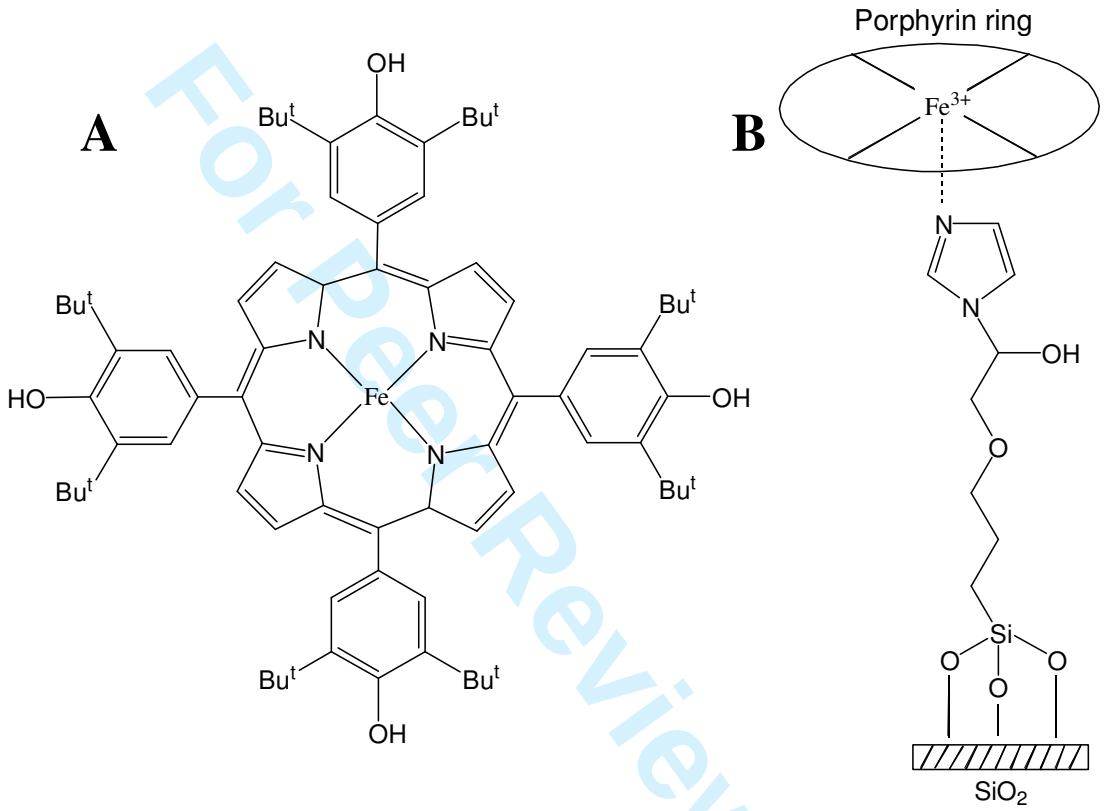

Scheme 1

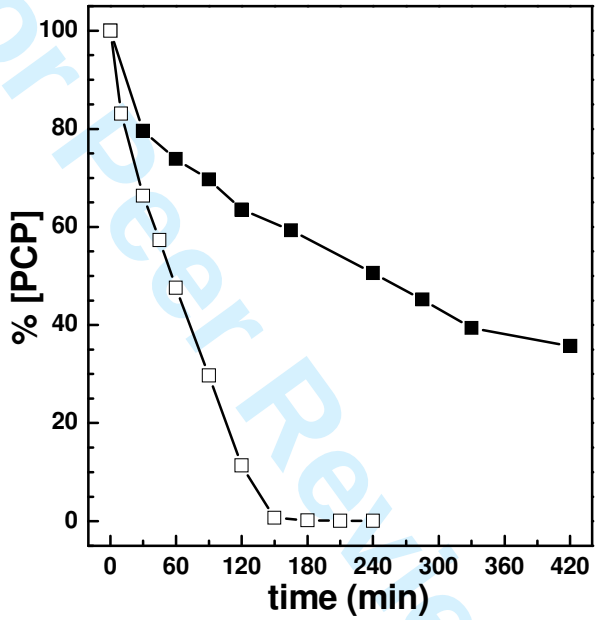

Figure 1

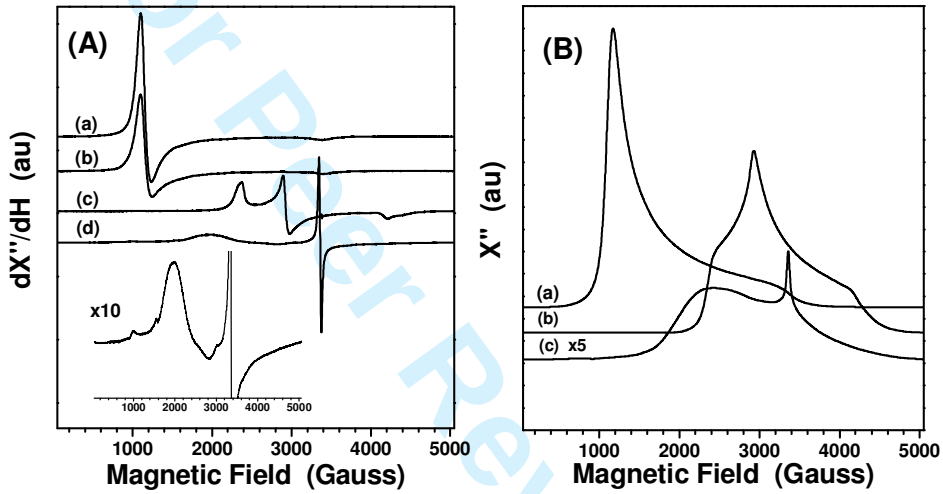

Figure 2

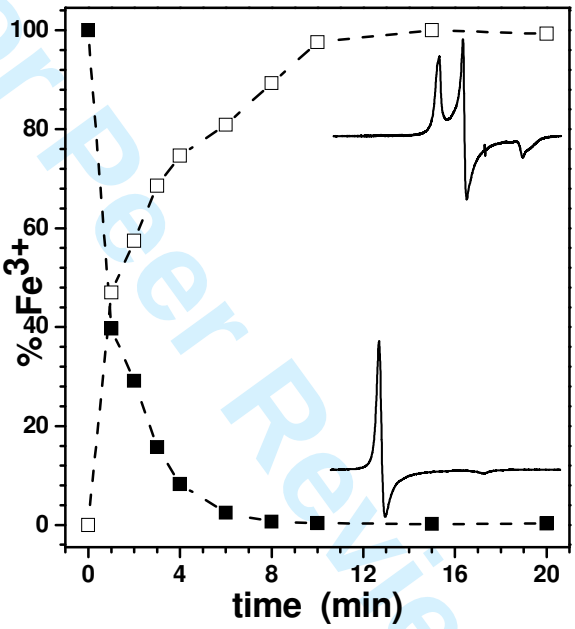

Figure 3

Table 1

Sample		g_x	g_y	g_z	Δ/λ	V/Δ	$a^2+b^2+c^2$	Σg^2
Cytochrome *c*-imidazole[a]		2.96	2.30	1.58	3.43	0.57	1.022	16.6
hemoglobin-imidazole[b]		2.91	2.26	1.53	3.32	0.58	1.002	15.9
A(Imid)$_2$	LS^A	2.858	2.305	1.56	3.01	0.67	1.003	15.9
	LS^B	2.850	2.285	1.60	3.40	0.63	1.004	15.9

g-values ±0.002

[a]Reference [49] [b]Reference [50].

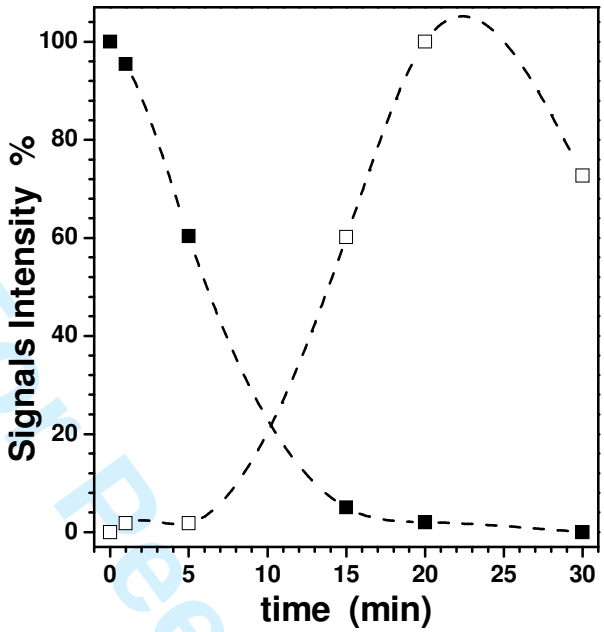

Figure 4

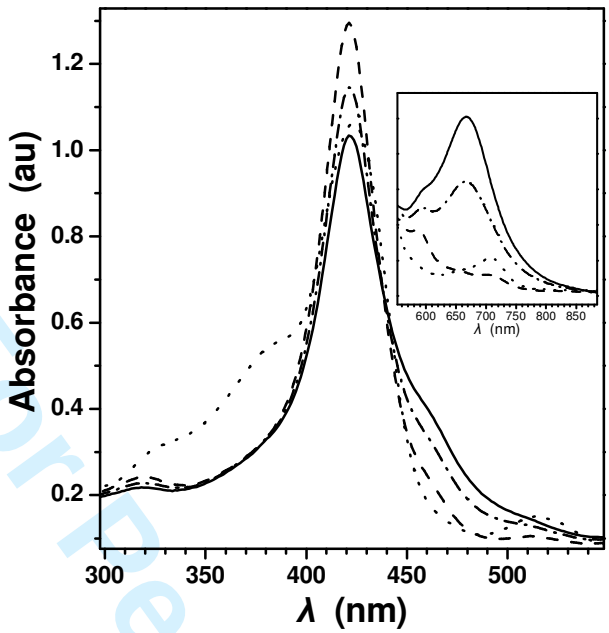

Figure 5

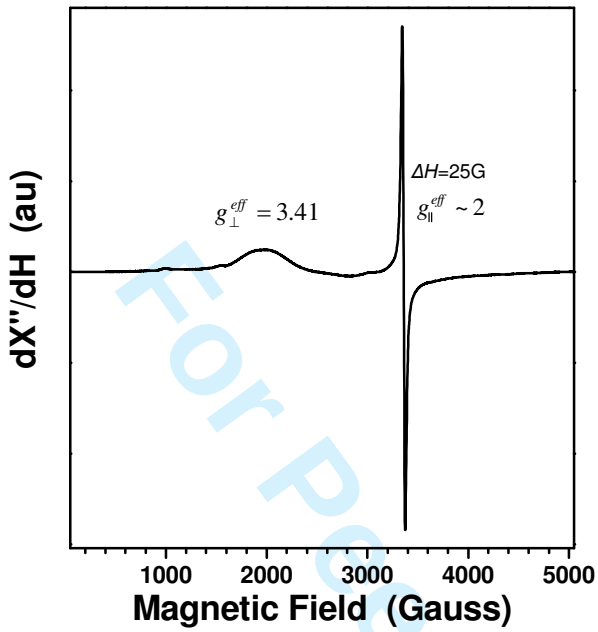

Figure 6

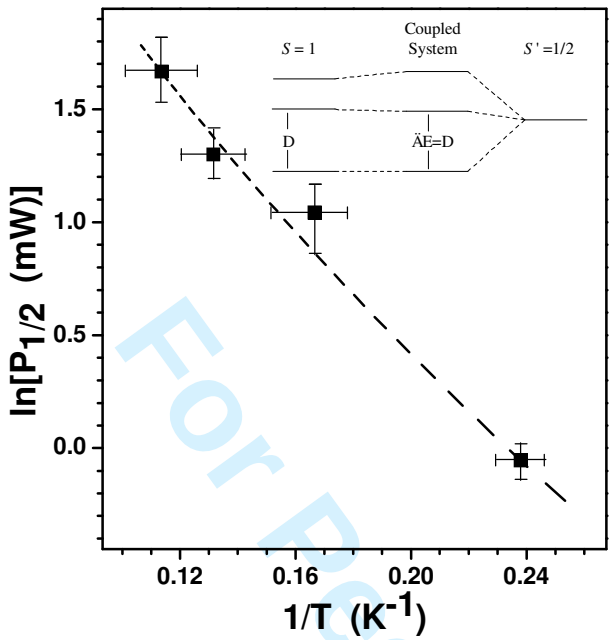

Figure 7

Table 2

Compound	*J/D*	*D* (cm^{-1})	*J*(cm^{-1})	Ref
A	0.31	11.5	+3.6	This work
Model Compounds				
Complex **1**	0.3	28	+8	43
Biological Systems				
HRP	≤+0.1	26	≤+2.6	19
LiP	0.29	33	–	17
CAT	0.4	–	–	47
ASP	0.28	–	–	44
CPO	-1.02	37	-38	20